In Turbulent Natural Convection in Enclosurers, Proc. Eurotherm Seminar N^o 22, pp. 43-53, Editions Europeennes Termique et Industrie, Eds: R.A.W.M. Henkes and C.J. Hoogendorf, Paris, 1993

COMPUTATION OF NATURAL-CONVECTION FLOW IN A SQUARE CAVITY

Lars Davidson

Thermo and Fluid Dynamics

Chalmers University of Technology

S-412 96 Gothenburg, Sweden

1 Abstract

The turbulent flow in a square cavity with $Ra = 5 \times 10^{10}$ is calculated using a finite-volume code based on SIMPLEC and staggered grid arrangements for the velocities. Two different differencing schemes are tested for the mean-flow equations: the hybrid upwind/central differencing scheme (first-order accuracy) and the QUICK scheme (third-order).

Wall-functions, low-Re $k-\varepsilon$ models and a two-layer $k-\varepsilon$ model are tested. Laminar solutions (i.e. $k = \nu_t \equiv 0$) were obtained with the low-Re models and the two-layer model.

The heat-flux term $\overline{v\theta}$ in the buoyancy terms in the k and ε-equations has been approximated in two different ways: the Boussinesq approximation, and the generalized gradient diffusion hypothesis.

The coefficient in front of the buoyancy term in the ε-equation should be 1 in vertical flow and 0 in horizontal flow. One way to achieve this is to multiply the coefficient with $\tanh|V/U|$. The influence of this modification is investigated.

2 The mean flow equations

The continuity, the momentum and the temperature equations are solved.

Although only the steady solutions are of interest in this study, the equations are solved in transient form, and the time step, Δt, is used as a free parameter by which the convergence rate may be optimized. The SIMPLEC solver of Van Doormaal and Raithby [1] has been used.

Two differencing schemes have been tested in the mean flow equations: the hybrid central/upwind [2] (first-order accuray) and the QUICK scheme (third-order accuray) by Leonard [3]. The exact form of the resulting coefficients in the discretized equations for a non-uniform grid are given in Ref. [4].

The hybrid upwind/central scheme was used in the k and ε-equations.

3 Turbulence models

3.1 The $k-\varepsilon$-equations

$$\frac{\partial \rho k}{\partial \tau} + \frac{\partial}{\partial x_j}\left(\rho U_j k\right) = \frac{\partial}{\partial x_j}\left[\left(\mu + \frac{\mu_t}{\sigma_k}\right)\frac{\partial k}{\partial x_j}\right] + P_k - \rho\varepsilon + G_k$$

$$\frac{\partial \rho \varepsilon}{\partial \tau} + \frac{\partial}{\partial x_j}\left(\rho U_j \varepsilon\right) = \frac{\partial}{\partial x_j}\left[\left(\mu + \frac{\mu_t}{\sigma_\varepsilon}\right)\frac{\partial \varepsilon}{\partial x_j}\right] + \frac{\varepsilon}{k}\left[c_{\varepsilon 1}\left(P_k + c_{\varepsilon 3} G_k\right) - c_{\varepsilon 2}\rho\varepsilon\right]$$

where

$$
\begin{aligned}
P_k &= \mu_t \frac{\partial U_i}{\partial x_j}\left(\frac{\partial U_i}{\partial x_j}+\frac{\partial U_j}{\partial x_i}\right) \\
G_k &= \rho\beta g\overline{v\theta} \qquad (1) \\
c_{\varepsilon 3} &= 1 \qquad (2)
\end{aligned}
$$

The constants have been assigned the values: $c_\mu = 0.09$, $c_{\varepsilon 1} = 1.44$, $c_{\varepsilon 2} = 1.92$, $\sigma_k = 1.0$, $\sigma_\varepsilon = 1.3$.

3.2 Buoyancy source terms

The usual way of treating the turbulent heat flux term in Eq. 1 is to use the Boussinesq approximation:

$$\overline{v\theta} = -\frac{\nu_t}{\sigma_t}\frac{\partial T}{\partial y} \qquad (3)$$

In vertical boundary layers this term is insignificant, since the magnitude of the vertical temperature gradient $\partial T/\partial y$ is small. Therefore Ince & Launder [5] introduced the generalized gradient diffusion hypothesis (GGDH) of Daly & Harlow [6] (also used in refs. [7, 8])

$$
\begin{aligned}
\overline{v\theta} &= -c_\theta \frac{k}{\varepsilon}\overline{vu_j}\frac{\partial T}{\partial x_j} \\
c_\theta &= 1.5\frac{c_\mu}{\sigma_t}
\end{aligned}
$$

Using Boussinesq approximation for the Reynolds stresses $\overline{vu_j}$ yields

$$\overline{v\theta} = c_\theta \frac{k}{\varepsilon}\left[\nu_t\left(\frac{\partial V}{\partial x}+\frac{\partial U}{\partial y}\right)\frac{\partial T}{\partial x}+\left(2\nu_t\frac{\partial V}{\partial y}-\frac{2}{3}k\right)\frac{\partial T}{\partial y}\right]$$

In a vertical boundary layer

$$
\begin{aligned}
\left|\frac{\partial V}{\partial x}\right| &\gg \left|\frac{\partial U}{\partial y}\right| \\
\frac{2}{3}k &\gg \left|2\nu_t\frac{\partial V}{\partial y}\right|
\end{aligned}
$$

and we get

$$\overline{v\theta} = \frac{3}{2}\frac{c_\mu}{\sigma_t}\frac{k}{\varepsilon}\nu_t\frac{\partial V}{\partial x}\frac{\partial T}{\partial x}-\frac{\nu_t}{\sigma_t}\frac{\partial T}{\partial y}$$

Note that the second term (which is not neglected) is the same as that in Eq. 3; the GGDH-term is thus written as:

$$\overline{v\theta} = \frac{3}{2}\frac{c_\mu}{\sigma_t}\frac{k}{\varepsilon}\nu_t\frac{\partial V}{\partial x}\frac{\partial T}{\partial x} \qquad (4)$$

3.3 Wall function

Tests were carried out using no wall functions, but setting $k = 0,\ \varepsilon = \infty$ at the wall. This did not succeed since the large value on ε was spread throughout the field during the iteration process. Instead standard wall functions [9] were used for k and ε, where u_* was obtained from the log-law for $y^+ > 11.63$ and otherwise from the linear law; the turbulence quantities at the node adjacent to the walls (n is the normal distance from the wall) were prescribed as

$$k = c_\mu^{-1/2} u_*^2,\ \varepsilon = \frac{u_*^3}{\kappa n}$$

3.4 Low-Reynolds-number $k - \varepsilon$ models

Some preliminar calculations were carried out using the Low-Re $k - \varepsilon$ models of Jones & Launder [10] and that of Davidson [11], but laminar flow fields (i.e. $k = \nu_t \equiv 0$) were obtained. Tests were performed calculating the heat flux in the buoyancy generation term G_k using either the Boussinesq approximation in Eq. 3 or the GGDH formula in Eq. 4, but laminar solutions were obtained for both cases.

3.5 Two-layer model

The two-layer model by Chen & Patel has been used [12, 13]. Near the walls the standard k equation is solved, and the turbulent length scale is prescribed as:

$$\ell_\mu = C_\ell n[1 - exp(-R_n/A_\mu)]$$

$$\ell_\varepsilon = C_\ell n[1 - exp(-R_n/A_\varepsilon)]$$

so that the dissipation term in the k-equation is obtained as:

$$\varepsilon = \frac{k^{3/2}}{\ell_\varepsilon}$$

and the turbulent viscosity as:

$$\mu_t = c_\mu \sqrt{k} \ell_\mu$$

The Reynolds number R_n and the constants are defined as

$$R_n = \frac{\sqrt{k} n}{\nu}$$

$$C_\ell = \kappa c_\mu^{-3/4},\ \ A_\mu = 70,\ \ A_\varepsilon = 2C_\ell$$

The one-equation model should be used near the walls for $R_n \leq 250$ [12], and the standard $k - \varepsilon$ model in the remaining part of the flow. The matching between the two models was taken at J-line $J = 10$ for the lower wall ($NJ - 10$ for the upper), and at $I = 20$ for the left (hot) wall ($NI - 20$ for the right wall). The location of the matching line was varied and the calculated results were found to be insensitive to the location of the matching line.

There are two advantages with two-layer models: unlike low-Re $k - \varepsilon$ models they can predict the flow in adverse pressure-gradient situations [12, 13], and they do not require as fine near-wall grids as do low-Re models. The latter require fine grids in order to resolve the steep gradients of ε.

4 The grid

A grid with 80×80 interior nodes is used, and it is generated using the equation

$$\begin{aligned} \frac{x_i}{H} &= \frac{1}{2}\left[1 + \frac{\tanh\left\{\alpha_1\left(i/i_{max} - \frac{1}{2}\right)\right\}}{\tanh\left(\alpha_1/2\right)}\right] \\ \frac{y_j}{H} &= \frac{j}{j_{max}} - \frac{1}{2\pi}\sin\left(2\pi\frac{j}{j_{max}}\right) \\ \alpha_1 &= 9.5 \end{aligned}$$

5 Results

The flow in a square cavity has been calculated for a Rayleigh number of $Ra = 5 \times 10^{10}$.

The local Nusselt number along the hot vertical wall is shown in Fig. 1 for two different $k-\varepsilon$ models (standard $k-\varepsilon$ using wall functions, and the two-layer $k-\varepsilon$ model), and two different differencing schemes (hybrid central/upwind and QUICK). It is seen that the different models give very different results. The two differencing schemes, however, give very similar results indicating a low numerical diffusion. This is not too suprising since numerical diffusion in lower-order schemes, such as the Hybrid scheme, mainly arises in regions where the flow is skew relative the grid lines. In the present cavity flow, the velocity vectors are in general aligned with the grid lines, especially in regions where convection is large (where it is important to use a more accurate differencing scheme such as QUICK).

In Figs. 2 and 3 the calculated V and T-profiles at $y/H = 0.5$ are presented.

From Figs. 1-3 it can be seen that the two-layer model gives no transition to turbulent boundary layer along the hot wall, and the problem with the two-layer model is thus the same as for the low-Re number $k-\varepsilon$ models: laminar solutions are obtained.

The remaining part of this section will be restricted to the presentation of results obtained with wall-functions and Hybrid differencing.

In Fig. 4 two modifications of the $k-\varepsilon$ model have been introduced. First, the G_k-term is calculated with the GGDH-expression in Eq. 4. The second modification is to sensitize the buoyancy term in the ε-equation to the flow direction. The $c_{\varepsilon 3}$-coefficient in Eq. 2 should vary between 0 in horizontal flow and 1 in vertical flow. This means that the coefficient should be dependent on the flow direction as

$$c_{\varepsilon 3} = \tanh|\frac{V}{U}| \tag{5}$$

When calculating the $c_{\varepsilon 3}$-coefficient from Eq. 5, the buoyancy term was calculated using the Boussinesq approximation in Eq. 3. No convergence was obtained with both modifications at the same time. From Fig. 4 it can be seen that the modification of the $c_{\varepsilon 3}$ does not affect the local Nu-number at all, whereas the GGDH approximation increases the local Nusselt number (the maximum local Nu at $x/H \simeq 0.1$ is increased by 10 %), and gives a small change in the point of transition.

It is illustrative to study the magnitude of the different terms in the turbulent kinetic energy equation. In Fig. 5 the dominant terms in the k-equation are shown near the hot wall for three different vertical stations. It can be seen that there are no drastic changes from $y/H = 0.2$ to $y/H = 0.7$, production being balanced by dissipation and diffusion. Everything occurs very close to the wall where $x^+ < 30$, which is inside the point of local velocity maximum. Inside this maximum

the velocity gradient is between one and two magnitudes larger than outside, which explaines the rapid deacay of turbulence in the outer part. It may be noted that the boundary layer in this square cavity is much thinner than that in tall cavities $H/L = 5$ where it extend well above $x^+ = 100$ [11].

In Fig. 5 it can further be seen that the contribution due to buoyancy – using the GGDH approximation – is negligible in the whole part of the boundary layer. Looking at its relative *local* importance, the situation changes, as depicted in Fig. 6. In the boundary-layer region inside the velociy maximum (for $x^+ < 30$) it is small and negative because $\partial V/\partial x > 0$ and $\partial T/\partial x < 0$. Outside the velocity maximum it becomes positive. The largest relative importance of the buoyancy term occurs at $x^+ \simeq 50$ for $y/H = 0.2$ and at $x^+ \simeq 100$ for $y/H = 0.5$ and 0.7 where it reaches values of 0.25-0.3.

The buoyancy terms calculated with Boussinesq approximation in Eq. 3 and GGDH hypothesis are compared in Fig. 7. It is seen that in the boundary layer the term obtained with the GGDH formula dominates. Close to the top of the cavity ($y/H = 0.99$), the term calculated with Boussinesq approximation becomes larger because here it is no longer true that the horizontal temperature gradient is much larger than the vertical one. For $x^+ > 25$ the horizontal gradient $|\partial T/\partial y|$ is larger than $|\partial T/\partial x|$, and further away from the wall at $x^+ \simeq 100$ it is one magnitude larger.

The dominant terms in the ε-equation are presented in Fig. 8 for two different vertical stations, $y/H = 0.5$ and $y/H = 0.99$. At $y/H = 0.5$ the qualitative picture is very similar as for the k-equation in Fig. 5b: the production is a source term and it is balanced by diffusion and dissipation. For the ε-equation, however, the dissipation term is slightly more important than in the k-equation, and the diffusion term is correspondingly smaller.

In Fig. 4 it was shown that the modification of the $c_{\varepsilon 3}$-coefficient according to Eq. 5 had no influence on the predicted local Nu-number. The tanh-function in Eq. 5 differs from 1 only when the U-velocity becomes comparable to V, which occurs in the corners of the cavity, see Figs. 9-10. Although the magnitude of G_k (using the Boussinesq approximation) attains its maximum ($x^+ \simeq 70$, see Fig. 7b) when the modification of $c_{\varepsilon 3}$ reaches its maximum (i.e. $\tanh|V/U| \to 0$), the influence of the modification is negligible because the $c_{\varepsilon 3}$-coefficient acts on a term which is negligible (see Fig. 8).

6 Conclusions

The buoyancy-driven flow in a square cavity with a Rayleigh number of 5×10^{10} has been calculated. Different treatments of the viscosity affected regions near the walls have been tested: wall-functions, low-Re $k-\varepsilon$ models and a two-layer $k-\varepsilon$. Laminar solutions (i.e. $k = \varepsilon \equiv 0$) were obtained with the low-Re models and the two-layer model.

Two different differencing schemes (Hybrid and QUICK) were tested for the mean-flow equations. Very similar results were obtained, which indicates that the numerical diffusion is small.

The standard expression for buoyancy terms in the k and ε-equation, based on Boussinesq approximation, contains the vertical temperature gradient $\partial T/\partial y$. In vertical boundary layers in natural-convection flow, this gradient is negligible compared with the horizontal temperature gradient. Using an alternative formulation, the generalized gradient diffusion hypothesis (GGDH) of Daly & Harlow [6], the horizontal gradient appears also. The influence of this modification has been investigated in the present study. It was found that GGDH buoyancy term increases the local Nusselt number (the maximum local Nu-number was increases by 10 %). The buoyancy term is negligible in the boundary layer inside the velocity maximum where production is balanced by diffusion and dissipation. In the outer part of the boundary layer the buoyancy term is locally up to 30 % of the largest term. The GGDH formula gives a much larger contribution than the Boussinesq approximation (orders of magnitude).

The influence of the buoyancy term in the ε-equation should be dependent on the flow direction,

and it should vanish when the flow is in the horizontal direction. A common way to deal with this problem in recirculating flows is to let the $c_{\varepsilon 3}$-coefficient be a function of the flow direction, i.e. $c_{\varepsilon 3} = \tanh|V/U|$. This modification of $c_{\varepsilon 3}$ was investigated using the Boussinesq approximation for the buoyancy term. It was found to have negligible influence on the flow compared to the $c_{\varepsilon 3} = 1$ case, simply because the buoyancy term with which the $c_{\varepsilon 3}$-coefficient is multiplied is negligible.

References

[1] J.P. Van Doormaal and G.D. Raithby, Enhancements of the SIMPLE Method for Predicting Incompressible Fluid Flows, *Numer. Heat Transfer*, **7**, 147-163, 1984.

[2] S.V. Patankar, *Numerical Heat Transfer and Fluid Flow*, McGraw-Hill, New York, 1980.

[3] B.P. Leonard, A Stable and Accurate Convective Modeling Based on Quadratic Upstream Interpolation, *Comp. Meth. Appl. Mech. Engng.*, Vol. 19, pp. 59-98, 1979.

[4] L. Davidson, Numerical Simulation of Turbulent Flow in Ventilated Rooms, PhD thesis, Dept. of Applied Thermodynamics and Fluid Mechanics, Chalmers University of Technology, Göteborg, 1989.

[5] N.Z. Ince and B.E. Launder, Computation of Turbulent Natural Convection in Closed Rectangular Cavities, Proc. 2nd *UK National Conference on Heat Transfer*, University of Strathclyde, Glasgow, Vol. 2, pp. 1389-1400, 1988.

[6] B.J. Daly and F.H. Harlow, Transport Equations of Turbulence, *Physics of Fluids*, Vol. 13, pp. 2634-2649, 1970.

[7] L. Davidson, Second-Order Corrections of the $k-\varepsilon$ Model to Account for Non-isotropic Effects due to Buoyancy, *Int. J. Heat Mass Transfer*, Vol. 33, No. 12, pp. 2599-2608, 1990.

[8] V. Shankar, L. Davidson and E. Olsson, Ventilation by Displacement: Calculation of the Flow in Vertical Plumes, ROOMVENT '92, Vol. 1, pp. 59-74, Sept. 2-4, Aalborg, 1992.

[9] W. Rodi, *Turbulence Models and their Application in Hydraulics*, International Association of Hydraulic Research, Monograph, Delft, 1980.

[10] W.P. Jones and B.E. Launder, The Prediction of Laminarization with a Two-Equation Model of Turbulence, *Int. J. Mass Heat Transfer*, Vol. 15, pp. 301-314, 1972.

[11] L. Davidson, Calculation of the Turbulent Buoyancy-driven Flow in a Rectangular Cavity Using an Efficient Solver and two Different Low Reynolds $k-\varepsilon$ Turbulence Models, *Numer. Heat Transfer*, Vol. 18, No. 2, pp. 129-147, 1990.

[12] H.C. Chen and V.C. Patel, Practical Near-Wall Turbulence Models for Complex Flows Including Separation, AIAA Paper No 87-1300, Honolulu, June 1987.

[13] L. Davidson and A. Rizzi, Navier-Stokes Computation of Airfoil in Stall Using Algebraic Reynolds-Stress Model, AIAA-paper 92-0195, Reno, 1992.

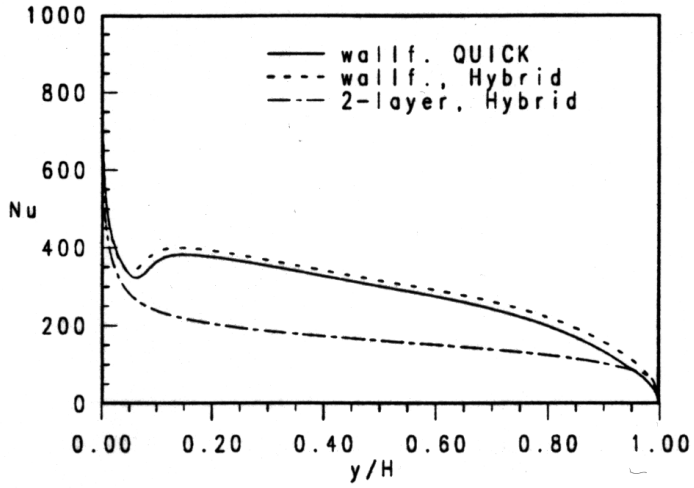

Fig. 1. Local Nusselt number along the hot wall at $Ra = 5 \cdot 10^{10}$. Three different cases are presented. 1: wall function with Hybrid scheme; 2: wall function with QUICK scheme; 3: two-layer model.

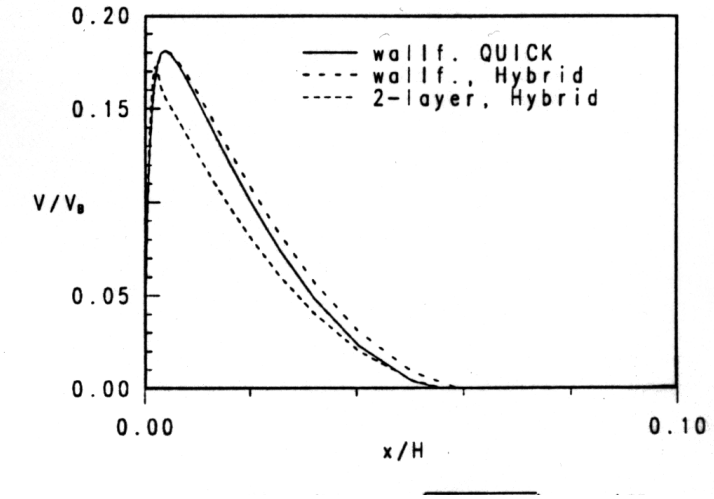

Fig. 2. V/V_B-velocities ($V_B = \sqrt{g\beta\Delta TH}$) at $y/H = 0.5$

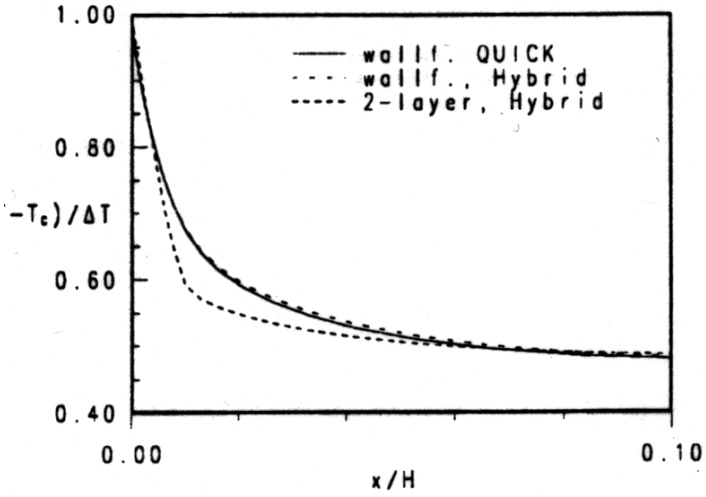

Fig. 3. T-profiles $(T - T_{cold})/\Delta T$ at $y/H = 0.5$

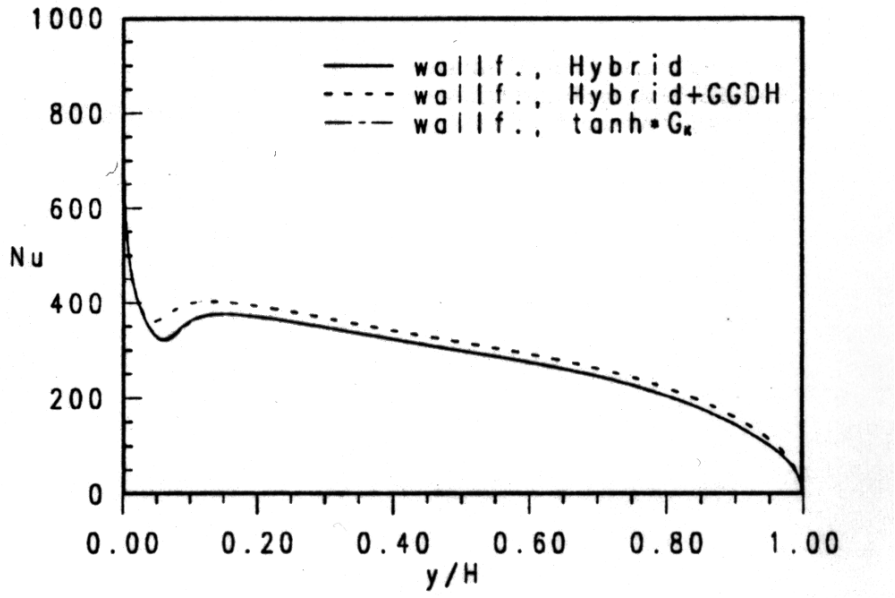

Fig. 4. Local Nusselt number along the hot wall. Three different cases are presented. 1: wall function with Hybrid scheme; 2: the buoyancy term G_k taken with the GGDH formula in Eq. 4; 3: the buoyancy term G_k in the ε-equation from Eq. 5

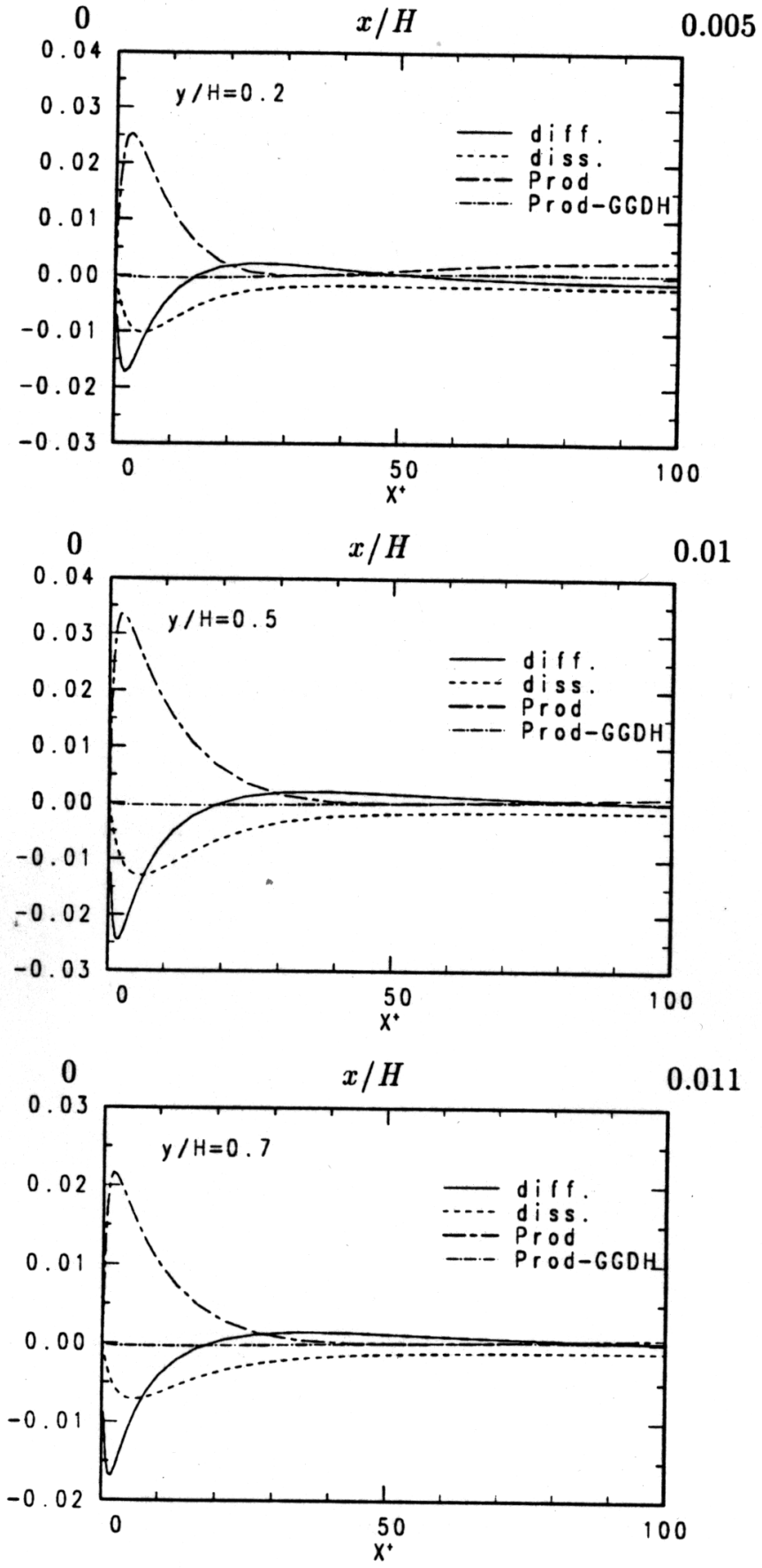

Fig. 5. Terms in the k equation near the hot wall at three different vertical stations. 1: diffusive term $\partial/\partial x\left[\left(\mu_t+\mu\right)\partial k/\partial x\right]$; 2: dissipation term $-\rho\varepsilon$; 3: production term P_k; 4: the buoyancy term G_k taken with the GGDH formula in Eq. 4.

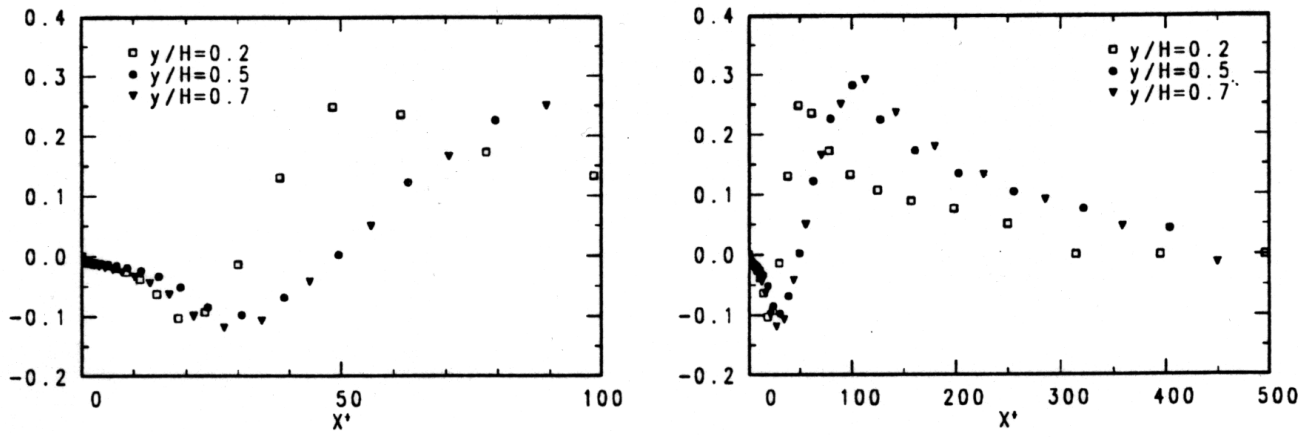

Fig. 6. The ratio of the buoyancy term G_k calculated with the GGDH formula in Eq. 4 and the largest of diffusion D_k, dissipation $\rho\varepsilon$ and produktion P_k, i.e. $G_k/\max\{|D_k|, P_k, \rho\varepsilon\}$.

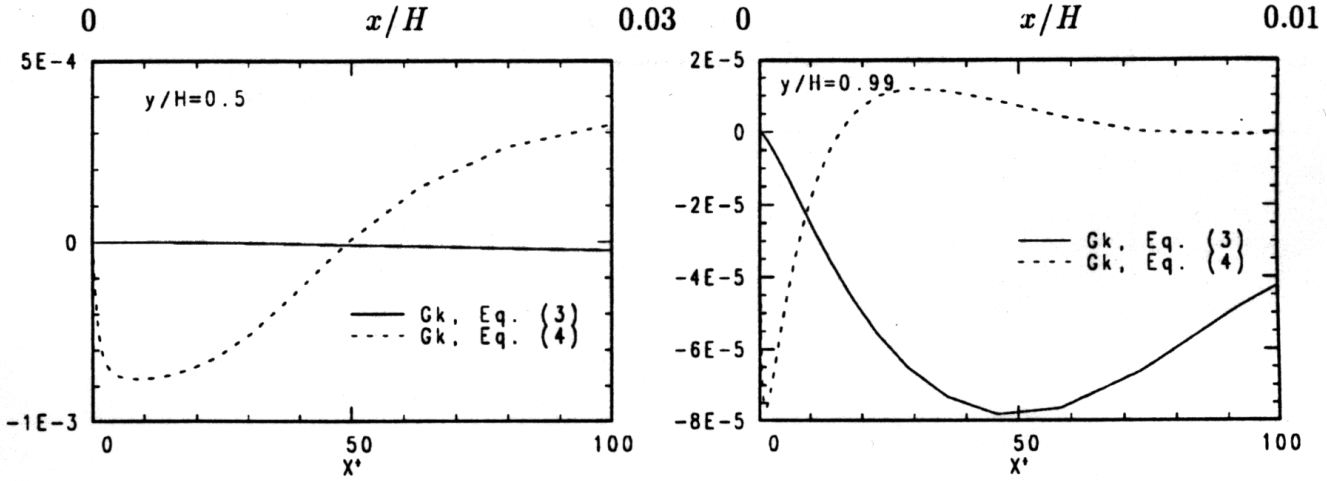

Fig. 7. Comparison of buoyancy terms G_k in k-equation. 1: Boussinesq approximation in Eq. 3; 2: GGDH formula in Eq. 4.

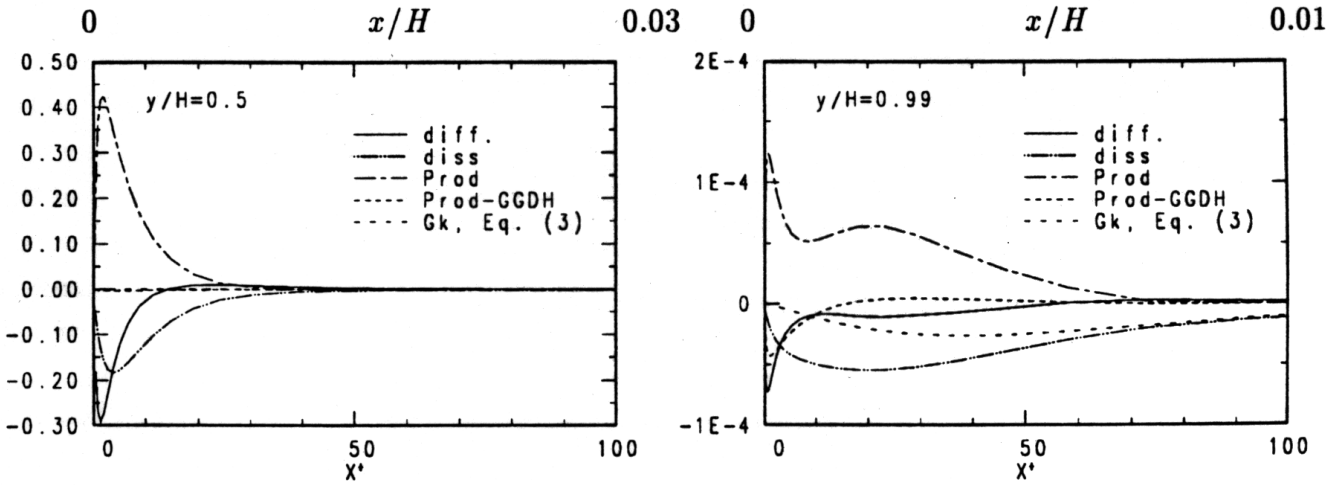

Fig. 8. Terms in the ε equation near the hot wall at two different vertical stations. 1: diffusive term $\partial/\partial x\left[(\mu_t/\sigma_\varepsilon+\mu)\,\partial\varepsilon/\partial x\right]$; 2: dissipation term $-c_2\rho\varepsilon^2/k$; 3: production term $c_1\varepsilon/kP_k$; 4: buoyant production term $c_2\varepsilon/kG_k$ from GGDH; 5: buoyant production term $c_2\varepsilon/kG_k$, Eq. 4.

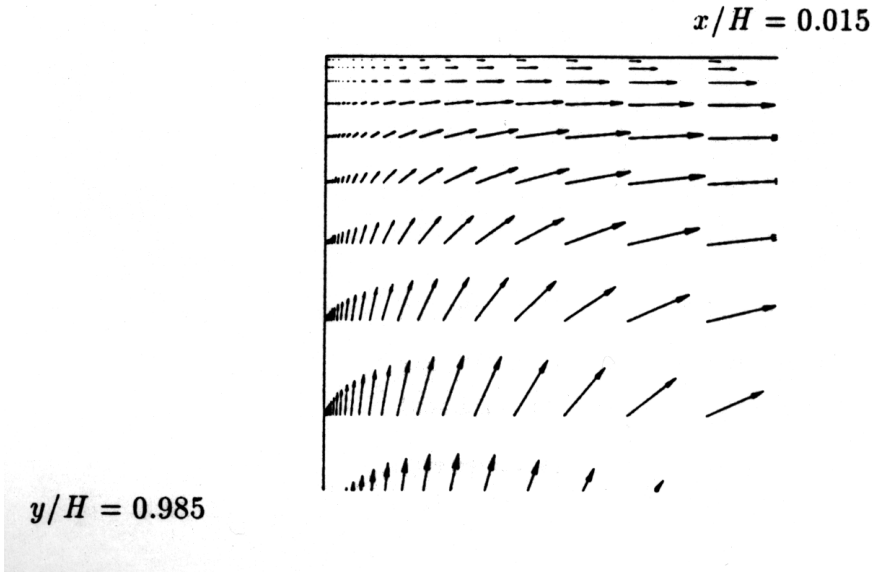

Fig. 9. Velocity vectors in the upper left (hot) corner of the cavity.

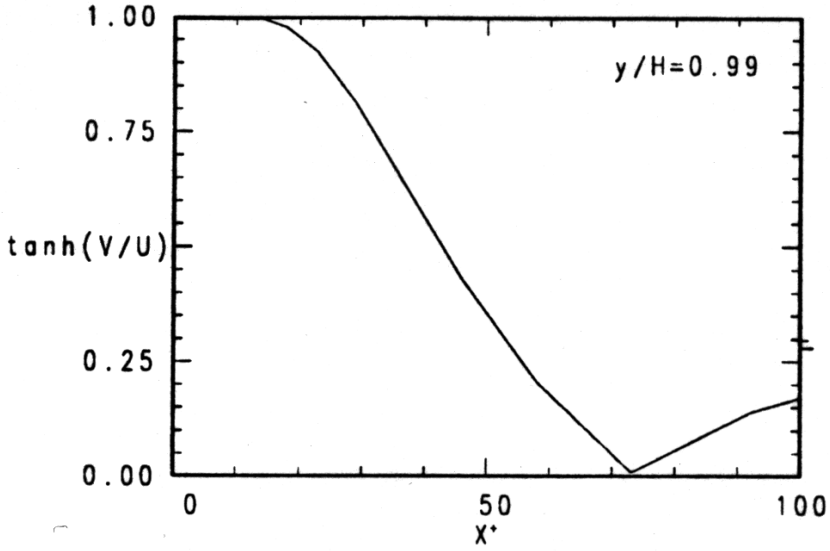

Fig. 10. The tanh-function used in the $c_{\varepsilon 3}$-coefficient in Eq. 5. $y/H = 0.99$.